Contents lists available at ScienceDirect

Regenerative Therapy

Original Article

Mastoid obliteration and external auditory canal reconstruction using 3D printed bioactive glass S53P4 /polycaprolactone scaffold loaded with bone morphogenetic protein-2: A simulation clinical study in rabbits

Fenghui Yu [1], Xiaoxia Fan [1], Hongxia Wu, Yangxi Ou, Xuxu Zhao, Tao Chen, Yi Qian, Houyong Kang[*]

Department of Otorhinolaryngology, The First Affiliated Hospital of Chongqing Medical University, Yixueyuan Road, Yuzhong District, Chongqing, China

ARTICLE INFO

ABSTRACT

Introduction: The lack of good prosthetic materials and objective standards has limited the promotion of mastoid obliteration and external auditory canal reconstruction, and the quality of the surgery varies. In this study, bioactive glass S53P4 (S53P4), the most popular artificial prosthetic material, was modified and combined with polycaprolactone (PCL) and bone morphogenetic protein-2 (BMP-2) to produce an individualized biological scaffold using 3D printing technology to explore a better material and method for mastoid obliteration and external auditory canal reconstruction.

Methods: 3D-printed S53P4/PCL scaffolds were fabricated from 3D reconstruction data of bone defect areas in New Zealand rabbits simulating "Canal Wall Down Mastoidectomy". The water absorption, swelling rate, porosity, and Young's modulus of the scaffold were measured, and the morphology and pore size of the scaffold were observed using scanning electron microscopy. The cytotoxicity of the S53P4/PCL scaffolds was detected using the CCK8 assay, and the in vitro antibacterial activity of the S53P4/PCL scaffolds was detected using the inhibition circle method. The BMP-2-loaded S53P4/PCL scaffolds were prepared using the drop-in lyophilization method and implanted into animal models. The biocompatibility, osteogenic activity, and external auditory canal repair of the scaffolds were observed using endoscopy, micro-CT, and histological examination.

Results: The S53P4/PCL scaffold was highly compatible with the defective area of the animal model, and its physicochemical properties met the requirements of bone tissue engineering. In vitro experiments showed that the S53P4/PCL scaffold was non-cytotoxic and exhibited better antibacterial activity than the same volume of the S53P4 powder. In vivo experiments showed that the S53P4/PCL scaffold had good biocompatibility and osteogenic activity, and could effectively repair bone defects and reconstruct the normal morphology of the external auditory canal in animal models. Furthermore, its osteogenic activity and repair ability were significantly improved after loading with BMP-2.

Conclusions: The 3D printed S53P4/PCL scaffold has great potential for clinical mastoid obliteration and external auditory canal reconstruction.

1. Introduction

Canal wall down mastoidectomy (CWDM) is widely used to treat middle ear diseases such as cholesteatoma and chronic otitis media because of its good surgical field exposure and reduced post-operative disease recurrence rate [1]. However, surgical removal of the mastoid and the posterior superior wall of the external auditory canal creates a large defective bony cavity, which leads to a series of

postoperative discomforts called "radicular cavity disease" [2]. Mastoid obliteration and external auditory canal reconstruction are effective solutions for these sequelae, and can reshape the mastoid and external auditory canal, promote postoperative epithelialization of the external auditory canal, and improve the quality of life of patients after surgery [3].

Currently, the most favored artificial bone repair material for clinical use in mastoid cavity filling is bioactive glass S53P4(S53P4) [4,5]. Studies have demonstrated that S53P4 has broad-spectrum antimicrobial properties [6,7], good biocompatibility and some plasticity [4,8]. However, its low bioactivity, slow in vivo degradation, mismatch between the rate of degradation and the rate of new bone production, and poor support of the external auditory canal wall does not meet the requirements for reconstructing the function of the external auditory canal [9].

Bone morphogenetic protein-2 (BMP-2) is an FDA-approved osteogenic protein used in the treatment of clinical bone defects. A recent study showed that BMP-2 does not only have strong osteogenic activity, but also a multi-cellular synergistic effect in the dynamic balance of osteogenesis and osteolysis; its loading into scaffold materials can coordinate the process of implant resorption and new bone formation [10].

Polycaprolactone (PCL) is mostly used as a scaffold-shaping material for loading bioactive factors or improving the mechanical properties of other materials because of its good biocompatibility, slow degradation rate, low acidic decomposition products compared to other polyesters, and good mechanical properties and plasticity [11].

In this study, we combined S53P3, PCL and BMP-2 to exploit their respective advantages; and fabricated S53P4/PCL scaffolds loaded with BMP2 using 3D printing technology; and implanted the scaffolds into animal models after simulated CWDM surgery; focusing on the osteogenic activity of the scaffold and the repair effect of the external ear canal.

2. Materials and methods

2.1. Materials

S53P4 (diameter 0—80 μm) was obtained from Kunshan Huaqiao Technology Materials Co., Ltd (Shuzhou, China). PCL (average molecular weight: 8000) was obtained from Kangrena Biotechnology Co., Ltd (Beijing, China). BMP-2 (25 μg/stem) was obtained from Nearshore Protein Co. Ltd (Shanghai, China). Further, 5-month-old New Zealand rabbits, (weight: 2.2—2.5 kg, cleanliness: normal grade) were provided by the Animal Experiment Center of Chongqing Medical University. All animal experiments were conducted according to the guidelines of the National Institute of Health Animal Care and the Animal Management Rules of the Ministry of Health of the People's Republic of China. The experimental protocol was approved by the Ethics Committee of the First Hospital of Chongqing Medical University (review batch number: 2021—634).

2.2. Fabrication of S53P4/PCL scaffold

One 5-month-old New Zealand rabbit was selected, and CT data of the preoperative auditory bulb area were obtained by CT scan (Fig. 1a). The outer 1/3 of the external auditory canal bone and the corresponding lateral wall bone of the auditory bulb area were removed to simulate CWDM and construct a CWDM animal model. Postoperative CT data for the auditory bulb area were obtained (Fig. 1b). The preoperative and postoperative imaging data were

intersected and differenced to obtain the three-dimensional data of the auditory bulb defect area (Fig. 1c). The 3D data of the auditory vesicle defect area were imported into the Bio-architect-SR software system to create a print model, and bio-ink (1.5 ml of deionized water + 2.8 g of PCL + 1.2 g of S53P4) was prepared according to the 3D printer system, heated to 80 °C, and stirred well. The S53P4/PCL stent was printed by fused deposition modeling (FDM) and stacked layer-by-layer according to the defect model of the auditory vesicle area (Fig. 1d).

2.3. Characterization of S53P4/PCL scaffolds

Three S53P4/PCL scaffolds were randomly selected, and the weight of the scaffolds was weighed and recorded as M1; a measuring cylinder was filled with 2 ml of anhydrous ethanol and recorded as V1; then, one scaffold was placed, the cylinder was sealed, the air was extracted, and the volume of the remaining liquid in the cylinder was recorded as V2; finally, the scaffold was removed, and the volume of the remaining liquid in the cylinder was recorded as V3.

$$\text{Porosity} = V1 - V3/V2 - V3 \times 100\%. \tag{1}$$

The scaffold was soaked in double distilled water for 24 h; after the scaffold fully absorbed water and swelled, the scaffold was removed weighed and labelled as M2; the volume of the scaffold was measured after swelling and labelled as V4.

$$\text{Water absorption rate} = M2\text{-}M1/M1 \times 100\% \tag{2}$$

$$\text{Swelling rate} = V4\text{-}(V2-V3)/(V2-V3) \times 100\% \tag{3}$$

Four square S53P4/PCL scaffolds with dimensions of 6 mm × 5 mm × 3 mm were fabricated (the materials used and the printing parameters were the same as the stents in the hearing bubble defect area), the Instron 5969 universal material testing machine was used, the static pressure measurement and movement speed of 0.3 mm/min were set, and the test data and process were recorded. In this experiment, the data of the first uniform deformation process in the range of strain rate <5%, removal of residual stress, and full contact were used to calculate Young's modulus.

One S53P4/PCL scaffold was randomly selected, quenched in liquid nitrogen, vacuum extracted, and gold plated; the surface of the stent and the microstructure of the truncated surface were observed at different magnifications under SEM, images were taken, and three randomly selected fields of view were used to analyze the morphological structure of the stent and calculate the pore size using Photoshop software.

2.4. CCK8 assay to detect cytotoxicity of S53P4/PCL scaffolds

The cellsexperiment were divided into S53P4/PCL + BMSCs and BMSCs control groups. First, 12 2 mm × 1 mm S53P4/PCL scaffolds were fabricated, sterilized, pre-wetted, and then placed in 24-well cell culture plates. The concentration of the BMSCs suspension was adjusted to 2×10^5/ml, and each scaffold was inoculated with 1 ml of cell suspension. The control group was treated in the same way. The specimens of the two groups were incubated at 37 °C, 5% CO2, and saturated humidity. Three samples were removed from each group on days 1, 3, 5, and 7 after inoculation, and 100 μl of CCK-8 solution was added to each sample, which was incubated in an incubator for 3 h. Next, 100 μl of liquid was added to each sample in
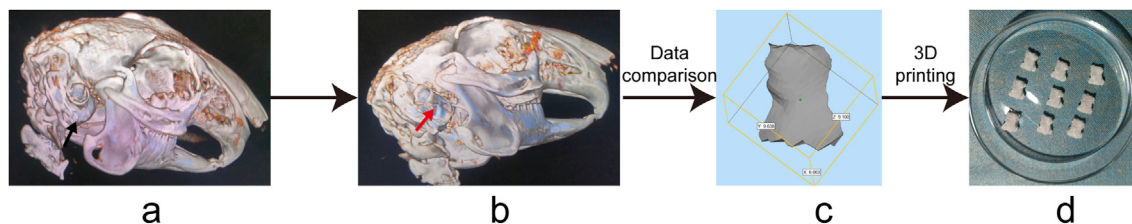
Fig. 1. Flow chart of preparation of S53P4/PCL scaffolds. a, The 3D reconstruction image of the preoperative specimen, the black arrow indicates the intact auditory vesicle area; b, The 3D reconstruction image of the postoperative specimen, the red arrow indicates the defect auditory vesicle area; c, The 3D reconstruction image of the auditory vesicle defect area; d, S53P4/PCL scaffolds.

a 96-well culture plate, and the absorbance value at 450 nm (OD) was measured using an enzyme marker.

Cell survival rate = (OD experimental group-OD blank medium)/ (OD control group-OD blank medium) × 100%.   (4)

2.5. Antibacterial properties of S53P4/PCL scaffolds were detected by the zone of inhibition method

Three 2 mm × 1 mm S53P4/PCL scaffolds were fabricated, and three S53P4 powders of the same volume were taken and sterilized by ultraviolet light for 3 h. *Staphylococcus aureus* was inoculated in the corresponding solid medium, standardized holes were made, the same volume of S53P4 powder and S53P4/PCL scaffold were embedded in the medium corresponding to the holes, the dishes were sealed with sealing film and incubated in a water-tight incubator at 37 °C for 5 days, and the size of the inhibition circle was measured.

2.6. Preparation of S53P4/PCL scaffolds loaded with BMP-2 by drip lyophilization

Refer to the methods of Niu [10] and Pelae [12]. Three S53P4/PCL scaffolds were randomly selected for animal experiments; 60 μg of BMP-2 was prepared in 100 μl of solution, and the BMP-2 solution was uniformly dripped onto the surface of the three spare scaffolds using a pipette gun and left to be fully absorbed, so that each scaffold was loaded with approximately 20 μg of BMP-2. The scaffolds were stored in a sealed and aseptic refrigerator at −20 °C overnight and lyophilized for use in animal experiments the following day.

2.7. S53P4/PCL scaffolds implanted in animals

Twelve New Zealand rabbits were selected according to the criteria and randomly divided into four groups: blank control, S53P4 powder, S53P4/PCL scaffold group, S53P4/PCL + BMP-2 scaffold group, with three rabbits in each group. Chloral hydrate (20%) was administered intravenously at the ear margin at a rate of 1 ml/kG body weight for anesthesia, ceftizoxime sodium 0.3 g was administered intramuscularly to the right thigh to prevent infection. The skin, subcutaneous tissue, and muscle of the auditory bulla area were incised; the bony external auditory canal and the lateral wall of the auditory bulla were exposed; the outer 1/3 of the external auditory canal and the bone of the lateral wall of the auditory bulla area were abraded; the bony structures were abraded as much as possible; the skin was kept intact; a bone defect area with the volume of the scaffold was created; and the corresponding repair material was implanted according to the grouping requirements. Auditory bulla specimens were obtained at 12 weeks after surgery.

2.8. Otolaryngoscopy

Endoscopic observation of the external auditory canal and tympanic membrane structure of fresh specimens, recording the morphological features of the ear canal, and focusing on the repair of the lateral wall of the external auditory canal.

2.9. Micro-CT scan

Micro-CT (VivaCT40) scans postoperative specimens for three-dimensional reconstruction of bone tissue, focusing on the morphology of the external auditory canal and the lateral wall of the auditory bulla. The bone defect area was selected as the region of interest (ROI) for analysis, and the total volume (TV) and new bone volume (BV) of the ROI were calculated using the system analysis software to calculate the new bone volume fraction (BVF), BVF=BV/TV.

2.10. Histological examination

The specimens were fully decalcified and paraffin-embedded, and six specimens were cut at the center. Three specimens were selected for hematoxylin and eosin (HE) staining, focusing on the inflammatory reaction of the new bone and surrounding tissues. The other three specimens were stained by Goldner trichrome staining, and Image-ProPlus 6.0 analysis software was used to calculate the trabecular area of the new bone and the total tissue area in the field of view. The percentage of trabecular bone area = trabecular bone area/total tissue area × %.

2.11. Statistical analysis

SPSS23.0 Statistical software was used for data processing and analysis, and the measurement data conformed to a normal distribution using the mean ± standard deviation (x ± s). A t-test was used for comparison of data between two groups. $P < 0.05$, and the difference was considered significant at $P < 0.01$ indicated a statistically significant difference.

3. Results

3.1. Characterization of S53P4/PCL scaffold

According to the 3D reconstruction data of the animal model defect area, the S53P4/PCL scaffold was successfully fabricated, of which S53P4 accounted for 30% and PCL accounted for 70%. The appearance of the stent was highly consistent with the defect area of the animal model, with an average volume coincidence rate of 93.4 ± 3.9% (Fig. 2). Three stents were randomly selected to measure the swelling rate of 7.5 ± 1.0%, the water absorption rate of 27.1 ± 1.4%, the porosity of 53.5 ± 1.6%, and the Young's modulus of 49.48 ± 3.71 MPa.

Fig. 2. S53P4/PCL scaffolds and Bone defect image.

The SEM images show that the S53P4 powder particles were uniform and in accordance with the expected material specifications (0−80 μm). The fibers on the scaffold surface were irregular, but the pores formed in each layer were interconnected. The cross section showed that the fibers in the scaffold were in regular shape and the pores in each layer were interconnected, with a transverse meridian of 112.3 ± 7.5 μm and a longitudinal meridian of 227.0 ± 15.5 μm (Fig. 3).

3.2. In vitro experiments

3.2.1. CCK8 assay to detect cytotoxicity of S53P4/PCL scaffolds

The proliferation activity of BMSCs in the S53P4/PCL scaffold medium was assessed using the CCK8 assay, which showed that the cell survival rate of the S53P4/PCL group was >90% at all time points compared to that of the control group, and the difference in OD values between the S53P4/PCL group and the control group was not statistically significant ($P > 0.05$) (Fig. 4).

3.2.2. Bacterial inhibition performance of S53P4/PCL scaffold

The results showed that the S53P4/PCL scaffold had stable antibacterial activity against *S. aureus*, and the diameter of the inhibition circle was significantly greater than that of the S53P4 powder at all time points; the difference was statistically significant ($P < 0.01$) (Fig. 5).

3.3. In vivo animal experiments

3.3.1. Postoperative animal condition and specimen appearance

All experimental animals healed well after the operation, and there were no adverse reactions, such as redness, purulence, and rejection in the auditory bubble area.

After 12 weeks, complete auditory bulla specimens were obtained, and endoscopic examination showed that the lateral wall of

the external auditory canal was obviously collapsed in the blank group, the lateral wall of the external auditory canal was uneven and locally trapped in the S53P4 powder group, and the external wall of the external auditory canal was smooth and well formed in the S53P4/PCL and S53P4/PCL + BMP-2 stent groups (Fig. 6).

3.3.2. Mirco-CT results

The 3D reconstruction of bone tissue showed that only a small amount of new bone was formed in the blank control group, and there was no significant repair of the bone defect. In the S53P4 powder group, the defect area was covered by S53P4 powder and its density value was comparable to that of the bone. In the S53P4/PCL group, new bone grew into the scaffold along the perimeter of the defective wound, with dense bone around the periphery and some flaky new bone formation near the center of the scaffold. In the S53P4/PCL + BMP-2 group, new bone formation was vigorous, with more new bone tissue growing into the scaffold along the perimeter of the defect and some new bone growth beyond the scaffold (Fig. 7a).

In the section of the external auditory canal of the specimen, it was observed that lateral wall of the external auditory canal of the blank control group had bone defects, the S53P4 powder group was partially repaired with an uneven surface, the S53P4/PCL group was smooth as a whole, but a small amount of defect was still unrepaired, and the S53P4/PCL + BMP-2 group healed well with a smooth appearance (Fig. 7a). The results of the metrological analysis showed that the S53P4/PCL + BMP-2 group had the highest volume of new bone, followed by the S53P4/PCL group, and the blank control group had only a small volume; the difference between the groups was statistically significant ($P < 0.05$) (Fig. 7b). The new bone volume fraction in the S53P4/PCL + BMP-2 group was higher than that in the S53P4/PCL group alone; the difference between the two groups was statistically significant ($P < 0.05$) (Fig. 7c). S53P4 powder CT density values were similar to bone, so
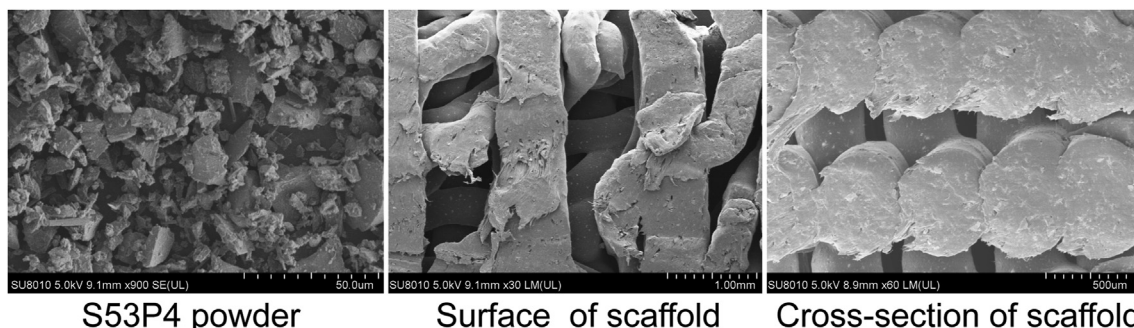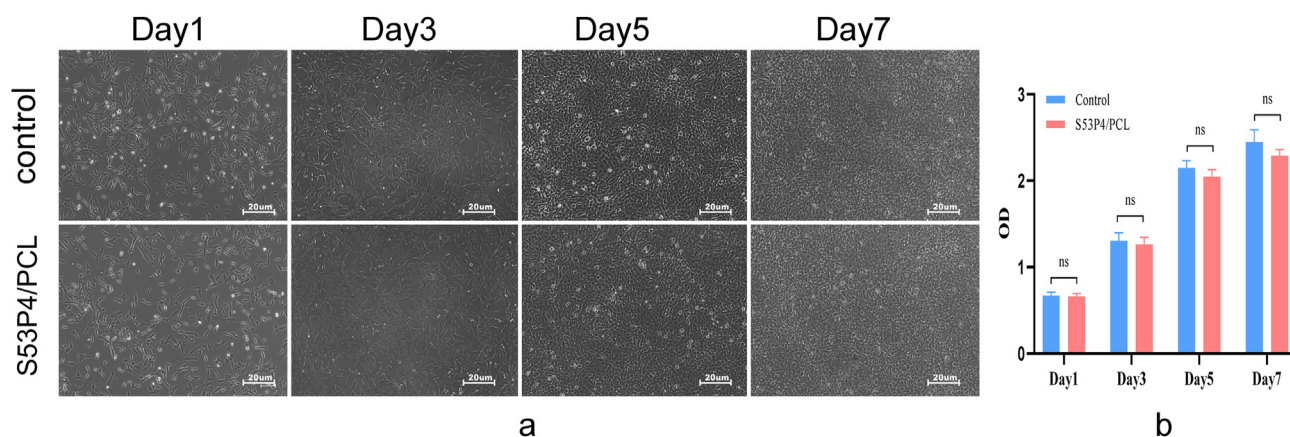

Fig. 3. SEM image of S53P4/PCL scaffolds.

Fig. 4. Cell proliferation activity of S53P4/PCL scaffolds detected by CCK8. a, Cell map of each node in the CCK8. b, Cell proliferation activity of S53P4/PCL scaffolds detected by CCK8 (n=3, ns P > 0.05).

micro-CTMirco-CT scans could not determine the new bone volume in this group of specimens and were not included in the analysis for discussion.

3.3.3. Histological analysis results

HE staining showed a little lymphocyte infiltration around the implanted scaffold or powder, and no obvious tissue necrosis was found. Goldner's trichrome staining showed that in the S53P4 powder group, new bone was formed around the powder packing, and part of it extended to the center, and no new bone was formed near the center of the powder. In the S53P4/PCL group, the new bone tissue around the scaffold obviously extended to the center of the scaffold, and there was more cartilage formation in the center of the scaffold, and scattered flaky new bone deposits were seen. In the S53P4/PCL + BMP-2 group, more new bone was formed around and at the center of the scaffold (Fig. 8a). Image-ProPlus 6.0 analysis software calculated the percentage of trabecular bone area, and the results showed that the S53P4/PCL + BMP-2 group was 42.9 ± 7.1, the S53P4/PCL group was 28.9 ± 3.7, and the S53P4 powder group was 14.4 ± 3.9. The differences between the two groups were statistically significant ($P < 0.05$) (Fig. 8b). The blank control group was not included in the histological analysis because of the absence of tissue in the bone-defect area.

4. Discussion

The major difference between CWDM compared to CWUM is the surgical excision of the posterior wall of the external auditory canal,
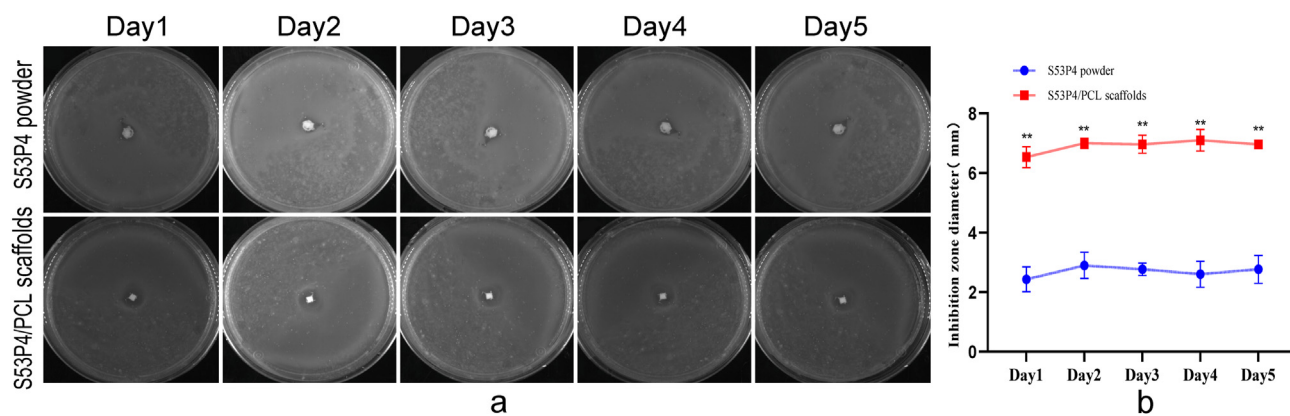

Fig. 5. Antibacterial function experiment of S53P4/PCL scaffold. a, Photo of inhibition zone of S53P4/PCL scaffolds. b, Measurement results of inhibition zone of S53P4/PCL scaffolds (n=3, ** P < 0.01).
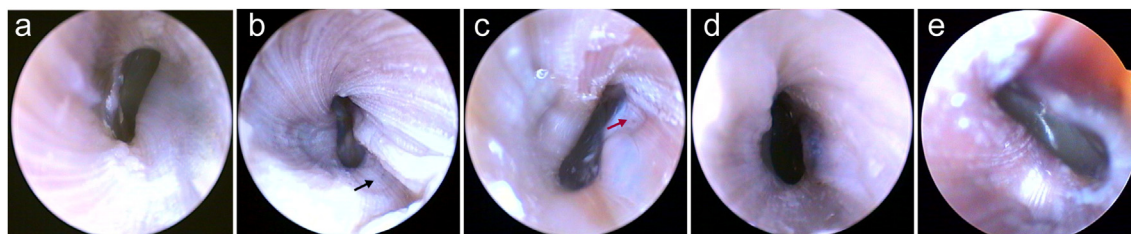
Fig. 6. Endoscopic images of auditory bubble specimens after operation. a, Healthy control group, the external auditory canal was smooth and in good shape; b, The black arrow indicates the collapse of the external auditory canal wall in the blank control group; c, The red arrow indicates the partial collapse of the external auditory canal wall in the S53P4 powder group;d e, The external auditory canal wall of the S53P4/PCL scaffold and the S53P4/PCL+BMP-2 scaffold group are smooth and in good shape.
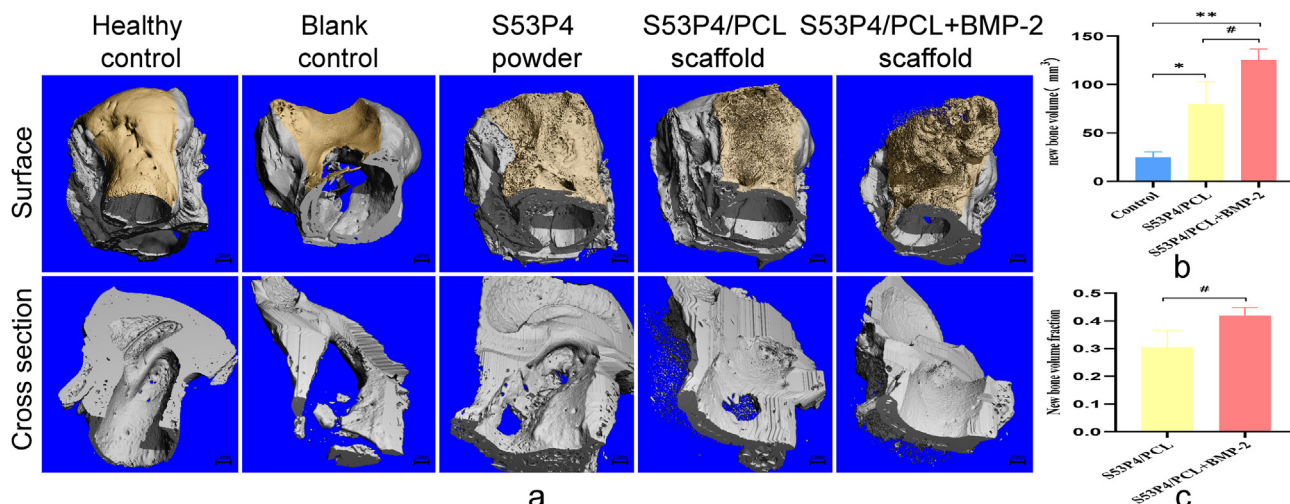
Fig. 7. Mirco-CT 3D reconstruction of postoperative specimens. a, The yellow area indicates the postoperative wound repair of the external auditory canal, and the lower part is the cross-sectional view of the external auditory canal. b c, Quantitative assessment of new bone volume(b) and volume fraction(c) in Mirco-CT scans (n=3, * # P < 0.05 , **P < 0.01).

which leaves the patient with a lack of normal postoperative external auditory canal structure, resulting in a series of complications [13]. Therefore, restoration of normal external auditory canal morphology is a key factor in postoperative mastoid cavity filling and external auditory canal reconstruction. We simulated the actual clinical situation and 3D printed S53P4/PCL scaffold using FDM technology was highly consistent with the animal model bone defect area in morphological appearance, which is a prerequisite to ensure morphological repair of the external auditory canal after surgery. Moreover, the modeling and fabrication process of this scaffold coincided with the clinical surgical treatment process. Therefore, the technique and process of this experiment can be directly applied in clinical treatment to perform 3D reconstruction of the temporal bone defect area of patients and produce individualized 3D printed scaffolds.

The porosity determines the biological and mechanical properties of the scaffold. Existing research shows that porosity between 35% and 75% is an excellent state that is more conducive to cell growth and considers the mechanical properties [14]. The porosity of the scaffold in our experiment was 53.5 ± 1.6%, which is in accordance with the above-mentioned range. As a non-load-

bearing bone, the temporal bone is close to important and fragile tissues such as the skull base, facial nerve, and inner ear. If implanting the mastoid with overly solid materials, it may cause damage to the above structures under the action of external force, resulting in serious consequences. The Young's modulus of the scaffold is 49.48 ± 3.71 MPa; its mechanical strength is comparable to that of trabecular bone of human vertebral (67 ± 45 MPa) [15]. Therefore, the scaffold not only does not threaten damage to the peripapillary tissue but also fully meets the mechanical requirements for supporting the morphology of the external auditory canal.

The pore size and intercommunication of scaffolds are other important factors affecting their biological properties, such as promoting the migration and proliferation of cells, facilitating the infiltration of blood vessels, improving the local nutritional and metabolic environment, and accelerating the process of bone repair [16–18]. Considering the influence of the size of the new blood vessels and the diameter of the new bone Haver's canal, the academic community generally believes that a minimum pore diameter of <100 μm is unfavorable for the ingrowth of blood vessels and the formation of new bone [19,20]. The transverse and
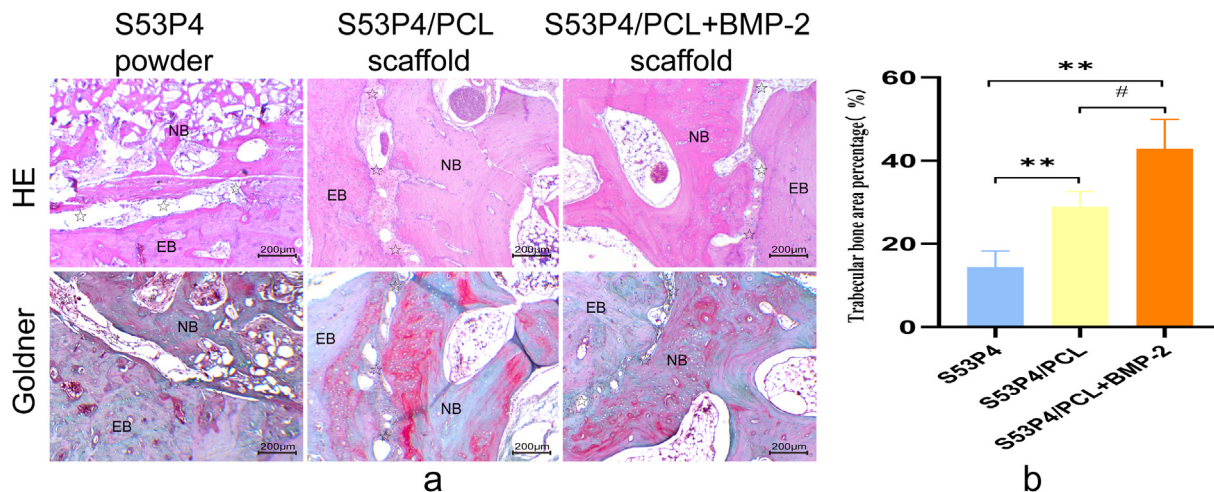
Fig. 8. Histological analysis of postoperative specimens. a, HE staining and Goldner trichrome staining picture (×40). EB, endogenous bone;NB,new bone; Black star, the border between the endogenous bone and the regenerated tissue. b, Goldner's trichrome stainings to determine the percentage of bone trabecular area (n=3, # P < 0.05 , **P < 0.01).

longitudinal meridians of the S53P4/PCL scaffolds fabricated in this study were all >100 μm, the fibers inside the scaffolds were well organized, and the pores of each layer were interconnected, which was fully beneficial to cell migration, blood vessel growth, and new bone formation. However, to meet the requirements of the morphological appearance of the scaffold, the fibers on the surface of the scaffold are disordered, and the formed pore size is irregular, which may affect the biological properties of the scaffold to a certain extent. This is a limitation of this study. In follow-up research, it is necessary to strengthen the rectification and optimize the 3D model route design for bracket printing.

Although both S53P4 and PCL are FDA-approved safe materials for clinical use, it is not known whether the scaffolds made from the combination of the two produce cytotoxic substances. We tested the results using the CCK8 assay and showed that the cell survival rate of the experimental group was >90% at all time points. The S53P4/PCL scaffolds were found to be noncytotoxic.

The broad-spectrum antibacterial activity of S53P4 is an important reason for its widespread use in clinical practice. Several studies have demonstrated significant bactericidal and antibacterial effects of S53P4 against a variety of aerobic bacteria, including methicillin-resistant *S. aureus* and anaerobic bacteria [6,7]. In this study, we found that the S53P4/PCL scaffold not only inherited the antibacterial activity of S53P4 but also showed superior antibacterial performance compared with the same volume of S53P4 powder, which was implanted in the body and released $Ca2+$, $Si4+$, and $Na +$ ions through its own degradation and increased local pH and osmotic pressure to achieve antibacterial activity [21,22]. We hypothesized that the composition of S53P4 in the composite scaffolds, although only 30% of its composition, and the interoperable pore size inside the scaffold greatly enhanced the surface area and diffusion ability of S53P4 to exchange with the surrounding fluids, and thus can exhibit superior antibacterial performance. This is one of the highlights of the present study.

In vivo experiments are an inevitable measure to verify the biological performance of scaffolds and the effectiveness of the procedure. In a previous study, Jang et al. [23—25] did a lot of research on introducing 3D printing technology into the field of mastoid obliteration. Composite scaffolds, such as PCL/alginate scaffolds and BP/MSCs/BMP2 scaffolds, have been fabricated and loaded with bioactive factors, such as rhBMP2 and umbilical cord serum, respectively, in an attempt to improve the biological properties of stents. The scaffolds were implanted into the auditory bulla cavity to observe biocompatibility and osteogenic activity, but the actual appearance and morphology of the mastoid obliteration and external auditory canal reconstruction were not evaluated, which simulates the CWDM to construct an animal model that is closer to the real clinical condition. The blank control group of New Zealand rabbits only had a little new bone formation and failed to heal naturally in the bone defect area after 12 weeks of natural growth. It proved that this model meets the requirements for "Critical Size Defect (CSD)" in bone tissue engineering [26,27], and is suitable for verifying the effect of bone defect repair. The surgical incisions of all experimental animals healed well after surgery. There were no adverse reactions such as swelling, suppuration and rejection in the auditory bulla area. No significant tissue necrosis and inflammatory reactions were observed in the HE-stained pathological examination of specimens from all groups. These results demonstrated the good biocompatibility of the implant material. The quantitative analysis of new bone on Mirco-CT and Goldner trichrome staining of bone trabeculae area ratio indicated that the S53P4/PCL + BMP-2 group had the most vigorous new bone formation, followed by the S53P4/PCL scaffold group, and the S53P4 powder group and the blank control group had only a little

new bone formation; this also proved again that the biological scaffold with interoperable pores can play the role of "bridge" and has good osteoconductivity to accelerate the repair of bone defects. Meanwhile, BMP-2 can induce migration, recruitment, differentiation and osteogenesis of osteoblasts based on the scaffolding effect, which can optimize the osteoinductivity of the scaffold and further promote bone defect repair [10].

Postoperatively, we focused on the repair of the external auditory canal. Both the endoscopic visualization and the Mirco-CT showed that the surface of the external auditory canal repaired by the S53P4 powder group was uneven and poorly formed, which reflects the problems that need to be solved. The simple S53P4 powder filling into the mastoid cavity does not have mechanical properties that support the morphology of the external auditory canal, which may lead to postoperative complications such as external auditory canal collapse, deformation, localized capsular pocket formation, and even implant leakage. Therefore, the external auditory canal is often shaped by taking auricular cartilage at the same time to improve its morphology [4,9], this may cause secondary damage to the donor location and increase the operation time.

The S53P4/PCL scaffold made in this experiment is highly compatible with the bone defect area due to its morphological appearance, sufficient mechanical properties, and interoperable mesh structure. New bone tissue formed after implantation into the bone defect area was induced to grow along the internal mesh structure of the scaffold, gradually covering the repair of the external auditory canal defect. The loaded BMP-2 protein further accelerates new bone formation, resulting in smooth and complete repair of the defective external auditory canal structure. However, we also noted that the mismatch between the rate of new bone tissue formation and the rate of scaffold degradation resulted in poor volume morphology of the new bone, especially in the S53P4/ PCL + BMP-2 group. Further adjustment and optimization are needed in subsequent studies to achieve better bone tissue repair.

5. Conclusions

The 3D-printed S53P4/PCL scaffold fabricated in this study is highly conformable to the animal model bone defect in morphology, has good biocompatibility and osteogenic activity, and exhibits better antibacterial activity than the same volume of S53P4 powder; it can effectively repair the animal model bone defect and reconstruct the normal morphology of the external auditory canal, its osteogenic activity and repair ability are significantly improved after loading BMP-2. The results of these studies may provide better repair materials and objective individualized solutions for clinical mastoid obliteration filling and external auditory canal reconstruction.

Author contributions

Feng-Hui Yu and Xiao-Xia Fan contributed equally to this study and were co-first authors. In this paper, Prof. Hou-Yong Kang was responsible for the design and guidance of the study; Feng-Hui Yu and Xiao-Xia Fan were responsible for the implementation of the experiments and writing of the paper. Tao Chen and Yi Qian were responsible for proofreading the paper. Xu—Xu Zhao,Hong-Xia Wu and Yang-Xi Ou assisted with some of the experiments.

Declaration of competing interest

The authors declare no conflicts of interest.

Acknowledgements

References

[1] Piras G, Sykopetrites V, Taibah A, Russo A, Caruso A, Grinblat G, et al. Long term outcomes of canal wall up and canal wall down tympanomastoidectomies in pediatric cholesteatoma. Int J Pediatr Otorhinolaryngol 2021;150: 110887. https://doi.org/10.1016/j.ijporl.2021.110887.

[2] Mehta RP, Harris JP. Mastoid obliteration. Otolaryngol Clin 2006;39(6): 1129—42. https://doi.org/10.1016/j.otc.2006.08.007.

[3] Weiss NM, Bächinger D, Botzen J, Großmann W, Mlynski R. Mastoid cavity obliteration leads to a clinically significant improvement in health-related quality of life. Eur Arch Oto-Rhino-Laryngol 2020;277(6):1637—43. https://doi.org/10.1007/s00405-020-05881-4.

[4] Sorour SS, Mohamed NN, Abdel Fattah MM, Elbary MEA, El-Anwar MW. Bioglass reconstruction of posterior meatal wall after canal wall down mastoidectomy. Am J Otolaryngol 2018;39(3):282—5. https://doi.org/10.1016/j.amjoto.2018.03.007.

[5] Skoulakis C, Koltsidopoulos P, Iyer A, Kontorinis G. Mastoid obliteration with synthetic materials: a review of the literature. J Int Adv Otol 2019;15(3): 400—4. https://doi.org/10.5152/iao.2019.7038.

[6] Munukka E, Leppäranta O, Korkeamäki M, Vaahtio M, Peltola T, Zhang D, et al. Bactericidal effects of bioactive glasses on clinically important aerobic bacteria. J Mater Sci Mater Med 2008;19(1):27—32. https://doi.org/10.1007/s10856-007-3143-1.

[7] Leppäranta O, Vaahtio M, Peltola T, Zhang D, Hupa L, Hupa M, et al. Antibacterial effect of bioactive glasses on clinically important anaerobic bacteria in vitro. J Mater Sci Mater Med 2008;19(2):547—51. https://doi.org/10.1007/s10856-007-3018-5.

[8] Leonard CG, McNally S, Adams M, Hampton S, McNaboe E, E Reddy C, et al. A multicenter retrospective case review of outcomes and complications of S53P4 bioactive glass. J Int Adv Otol 2021;17(3):234—8. https://doi.org/10.5152/iao.2021.9053.

[9] Król B, Cywka KB, Skarżyńska MB, Skarżyński PH. Mastoid obliteration with S53P4 bioactive glass after canal wall down mastoidectomy: preliminary results. Am J Otolaryngol 2021;42(2):102895. https://doi.org/10.1016/j.amjoto.2020.102895.

[10] Niu H, Ma Y, Wu G, Duan B, Wang Y, Yuan Y, et al. Multicellularity-interweaved bone regeneration of BMP-2-loaded scaffold with orchestrated kinetics of resorption and osteogenesis [published correction appears in Biomaterials. 2019;216:119216. https://doi.org/10.1016/j.biomaterials.2019.05.027. 2021 Jan;264:120376].

[11] Yang X, Wang Y, Zhou Y, Chen J, Wan Q. The application of polycaprolactone in three-dimensional printing scaffolds for bone tissue engineering. Polymers 2021;13(16): 2754. https://doi.org/10.3390/polym13162754. Published 2021 Aug 17.

[12] Pelaez M, Susin C, Lee J, Fiorini T, Bisch FC, Dixon DR, et al. Effect of rhBMP-2 dose on bone formation/maturation in a rat critical-size calvarial defect model. J Clin Periodontol 2014;41(8):827—36. https://doi.org/10.1111/jcpe.12270.

[13] Lucidi D, De Corso E, Paludetti G, Sergi B. Quality of life and functional results in canal wall down vs canal wall up mastoidectomy. Acta Otorhinolaryngol Ital 2019;39(1):53—60. https://doi.org/10.14639/0392-100X-2005.

[14] Duan B, Wang M, Zhou WY, Cheung WL, Li ZY, Lu WW. Three-dimensional nanocomposite scaffolds fabricated via selective laser sintering for bone tissue engineering. Acta Biomater 2010;6(12):4495—505. https://doi.org/10.1016/j.actbio.2010.06.024.

[15] Wang X, Xu S, Zhou S, Xu W, Leary M, Choong P, et al. Topological design and additive manufacturing of porous metals for bone scaffolds and orthopaedic implants: a review. Biomaterials 2016;83:127—41. https://doi.org/10.1016/j.biomaterials.2016.01.012.

[16] Knychala J, Bouropoulos N, Catt CJ, Katsamenis OL, Please CP, Sengers BG. Pore geometry regulates early stage human bone marrow cell tissue formation and organisation. Ann Biomed Eng 2013;41(5):917—30. https://doi.org/10.1007/s10439-013-0748-z.

[17] Xue W, Krishna BV, Bandyopadhyay A, Bose S. Processing and biocompatibility evaluation of laser processed porous titanium. Acta Biomater 2007;3(6): 1007—18. https://doi.org/10.1016/j.actbio.2007.05.009.

[18] Van Bael S, Chai YC, Truscello S, Moesen M, Kerckhofs G, Van Oosterwyck H, et al. The effect of pore geometry on the in vitro biological behavior of human periosteum-derived cells seeded on selective laser-melted Ti6Al4V bone scaffolds. Acta Biomater 2012;8(7):2824—34. https://doi.org/10.1016/j.actbio.2012.04.001.

[19] Elbary MEA, Nasr WF, Sorour SS. Platelet-rich plasma in reconstruction of posterior meatal wall after canal wall down mastoidectomy. Int Arch Oto-rhinolaryngol 2018;22(2):103—7. https://doi.org/10.1055/s-0037-1602694.

[20] Faramarzi M, Kaboodkhani R, Faramarzi A, Roosta S, Erfanizadeh M, Hosseinialhashemi M. Mastoid obliteration and external auditory canal reconstruction with silicone block in canal wall down mastoidectomy. Laryngoscope Investig Otolaryngol 2021;6(5):1188—95. https://doi.org/10.1002/lio2.672. Published 2021 Sep. 27.

[21] Gonzalez Moreno M, Butini ME, Maiolo EM, Sessa L, Trampuz A. Antimicrobial activity of bioactive glass S53P4 against representative microorganisms causing osteomyelitis - real-time assessment by isothermal microcalorimetry. Colloids Surf B Biointerfaces 2020;189:110853. https://doi.org/10.1016/j.colsurfb.2020.110853.

[22] Zhang D, Leppäranta O, Munukka E, Ylänen H, Viljanen MK, Eerola E, et al. Antibacterial effects and dissolution behavior of six bioactive glasses. J Biomed Mater Res 2010;93(2):475—83. https://doi.org/10.1002/jbm.a.32564.

[23] Jang CH, Cho GW, Song AJ. Effect of bone powder/mesenchymal stem cell/ BMP2/fibrin glue on osteogenesis in a mastoid obliteration model. Vivo 2020;34(3):1103—10. https://doi.org/10.21873/invivo.11881.

[24] Jang CH, Kim W, Kim G. Effects of fibrous collagen/CDHA/hUCS biocomposites on bone tissue regeneration. Int J Biol Macromol 2021;176:479—89. https://doi.org/10.1016/j.ijbiomac.2021.02.050.

[25] Jang CH, Kim MS, Cho YB, Jang YS, Kim GH. Mastoid obliteration using 3D PCL scaffold in combination with alginate and rhBMP-2. Int J Biol Macromol 2013;62:614—22. https://doi.org/10.1016/j.ijbiomac.2013.10.011.

[26] Beederman M, Lamplot JD, Nan G, Wang J, Liu X, Yin L, et al. BMP signaling in mesenchymal stem cell differentiation and bone formation. J Biomed Sci Eng 2013;6(8A):32—52. https://doi.org/10.4236/jbise.2013.68A1004.

[27] Wu M, Li YP, Zhu G, Lu Y, Wang Y, Jules J, et al. Chondrocyte-specific knockout of Cbfβ reveals the indispensable function of Cbfβ in chondrocyte maturation, growth plate development and trabecular bone formation in mice. Int J Biol Sci 2014;10(8):861—72. https://doi.org/10.7150/ijbs.8521. Published 2014 Jul 29.